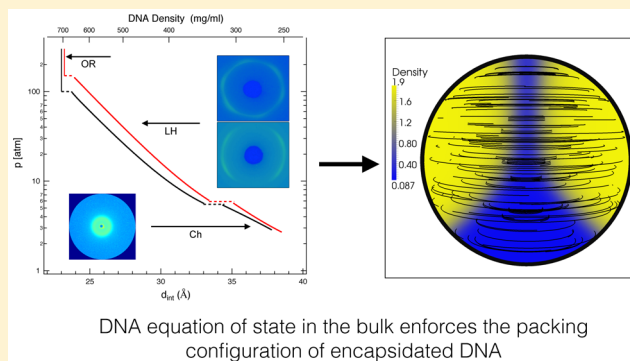


DNA Equation of State: In Vitro vs In Viro

Rudolf Podgornik,^{*,†,‡,§} M. Alphan Aksoyoglu,[†] Selcuk Yasar,[†] Daniel Svenšek,[§] and V. Adrian Parsegian[†][†]Department of Physics, University of Massachusetts, Amherst, Massachusetts 01003, United States[‡]Department of Theoretical Physics, Jožef Stefan Institute, SI-1000 Ljubljana, Slovenia[§]Department of Physics, Faculty of Mathematics and Physics, University of Ljubljana, SI-1000 Ljubljana, Slovenia

ABSTRACT: We formulate a continuum approach to the equation of state (density dependence of osmotic pressure) of bulk DNA and encapsidated DNA, as well as review the phase diagram of DNA in the regime of densities relevant for DNA packing in bacteriophages. We derive the first integral of the equilibrium equations that connects the behavior of DNA in the bulk and in nanoscale enclosures, and we delineate the changes wrought upon the mesophase equilibria of encapsidated DNA. We show how multiphase equilibria and complicated spatial distribution of DNA density and orientation can emerge due to the curvature contribution to the DNA osmotic pressure within the capsid.



DNA equation of state in the bulk enforces the packing configuration of encapsidated DNA

I. INTRODUCTION

In vitro, long and short DNA in solutions exhibit a sequence of ordered liquid-crystalline mesophases^{1,2} when there is an increase in the DNA density,^{3–9} resulting in different forms of DNA compaction in the biological milieu, characterized by similar DNA lengths and densities, bathing solution conditions, and osmotic pressures.^{10–13} These compacted forms of DNA in the biological environment include most importantly the DNA packing within bacteriophage capsids^{14,16–20} at osmotic pressures exceeding 50 atm and at densities within the regime of highly concentrated DNA solutions.^{21–25} The study of these compacted forms of DNA is thus not only relevant from the fundamental biophysics point of view but also illuminates the molecular mechanisms of DNA packing in bacteriophages, as well as constraints to the possible mechanisms of gene delivery.^{21,22,26} The general outlines of the DNA phase diagram in bulk solutions displays a progressive ordering phase sequence: isotropic (I) → cholesteric (Ch) → line hexatic (LH) (or hexagonal columnar H) → orthorhombic (OR); however, many details, including the complete fragment length dependence^{8,9} and the demarcation between the line hexatic and hexagonal order, remain to be systematically investigated.

Packing of viral DNA in viro¹⁵ such as in bacteriophages T7,¹⁶ T4,¹⁷ epsilon15,^{20,27} P22,¹⁹ and ϕ 29,^{18,28,29} provides a detailed picture of the genome organization inside bacteriophage proteinaceous capsids. At densities corresponding to full packing, DNA appears to be wrapped into a coaxial *inverse spool*, characterized by orientational ordering and high packing density close to the capsid wall that both appear to decay toward the center of the capsid characterized by a depletion hole. In contrast, the T5 bacteriophage DNA appears to show a more complicated ordered structure, exhibiting mesophase domains without a fully developed inverse spool symmetry.^{30,31}

Faced with the structural details of the packing of DNA inside bacteriophage capsids, an evident question is in what way(s) a confining proteinaceous enclosure interferes with the order exhibited by DNA in the bulk solution at nominally the same bathing conditions. A mesoscale continuum approach, based on the physics of liquid crystals,^{32–35} allows us to connect the two and to derive some general consequences that can guide our detailed understanding of the genome packing in bacteriophages.

II. RESULTS

A. DNA Phase Diagram. We limit ourselves to the consideration of monovalent salt bathing solutions exclusively.³⁶ Long Na-DNA in solutions above 650 mg/mL (or above ~90% relative humidity) is in an orthorhombic (OR) crystalline phase³⁷ and in A-form conformation with a helical pitch of ~2.9 nm (~3.4 nm for B-form).³⁸ Short(er) 50 nm Na-DNA fragments are in the OR phase above 670 mg/mL but do not show the A-form fingerprint.⁸ In the OR phase, the DNA density appears to remain unchanged upon further drying below 90% relative humidity.³⁸ Lower density osmotic stress experiments, in which the osmotic pressure is tightly controlled,^{39–41} indicate that long DNA solutions are in the line hexatic (LH) mesophase, characterized by long-range orientational and bond orientational orders⁴² and short-range positional order.^{12,43} The OR → LH transition at osmotic pressure ~170 atm is characterized by a discontinuous DNA density change as well as the first-order X-ray diffraction peak

Special Issue: William M. Gelbart Festschrift

Received: February 26, 2016

Revised: April 7, 2016

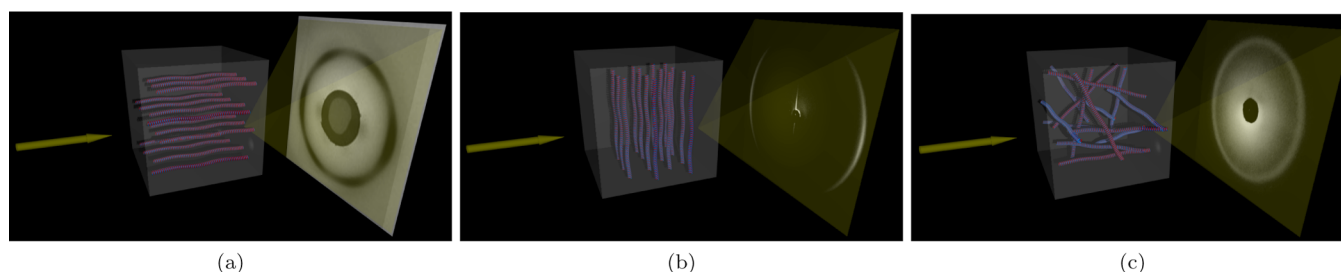


Figure 1. Appearance of a 6-fold symmetric azimuthal intensity profile of the first-order X-ray diffraction peak for the oriented DNA suggests that long-fragment DNA packs in a straight parallel untwisted arrangement in the LH phase,¹² with long-range bond-orientational order perpendicular to the axis of the molecules. (a) X-ray oriented parallel and (b) perpendicular to the average director. Disordered Ch phase gives a liquid-like circular diffraction pattern (c). Direction of incident X-ray beam is indicated by the arrow.

broadening, with the appearance of a 6-fold symmetric azimuthal scattering intensity profile at lower densities,^{12,37} Figure 1. Na-DNA remains in the LH phase over the whole interval of 650–350 mg/mL, while short(er) 50 nm Na-DNA fragments show a different phase sequence, being in 3D hexagonal columnar phase below 670 mg/mL with progressive disordering to a 2D hexagonal columnar phase at 380 mg/mL.⁸ Besides the LH, the other important DNA mesophase at densities relevant for capsid packing is the cholesteric (Ch) phase,⁴⁴ characterized by a much broader diffraction peak than in the LH phase, indicating strong conformational fluctuations. The LH → Ch transition is also characterized by a discontinuous change in the DNA density at osmotic pressure ~6 atm and DNA density 300 mg/mL and thus appears to be of first-order.³⁷ The Ch phase then extends to concentrations of ~13 mg/mL when DNA finally enters into the isotropic phase.⁴⁵ In both, the Ch and LH phases, DNA is organized in a lattice with local hexagonal symmetry,⁴⁶ with the bond orientational order in the Ch phase being short-range, while it becomes macroscopic in the LH phase.⁴⁷ This implies that the long-fragment DNA packs in a straight parallel untwisted arrangement in the LH phase, exhibiting long-range bond-orientational order in the directions perpendicular to the ordered axes of the molecules.^{12,43} Very short fragment B-form DNA oligomers of 6 to 20 base pairs in length have been shown to exhibit isotropic, hexagonal columnar liquid crystal phases and crystal phases, with increasing DNA concentration.⁵

The positional order in both phases, LH and Ch, for long-fragment DNA thus remains liquid-like, i.e., short-range (unlike in the case of short fragment DNA⁸), the bond orientational order and the local positional ordering change abruptly at the transition between these two phases, exhibiting all the characteristics of a discontinuous, first-order transition.³⁷ This discontinuous transition in univalent NaCl solution also bears some resemblance to the DNA condensation transition in polyvalent salts,^{48,49} such as CoHex, at subcritical concentrations, that thus bears some similarity to the Ch → LH transition in NaCl solutions.

B. In Vitro Equation of State. The in vitro equation of state (EOS) relates the osmotic pressure, p , with density, ρ , in a bulk DNA solution.⁵⁰ EOS depends on temperature (T), concentration (n), and salt type (i) of the bathing solution, and can be written as

$$p = p_0(\rho; T, n_i) \quad (1)$$

The index 0 refers to the bulk. Since osmotic stress experiments are done in equilibrium with a bulk salt reservoir, i.e., at a constant chemical potential of all the salt species, n_i is just

short-hand for the chemical potential of the various salt types in the bulk.³⁹ The EOS of DNA contains different contributions in different parts of its phase diagram.^{37,50} Furthermore, the details of the EOS of DNA depend strongly on the type of the ions in the bathing solution.⁵¹ Even exchanging Na for Li, see Figure 2, has an important quantitative effect on osmotic

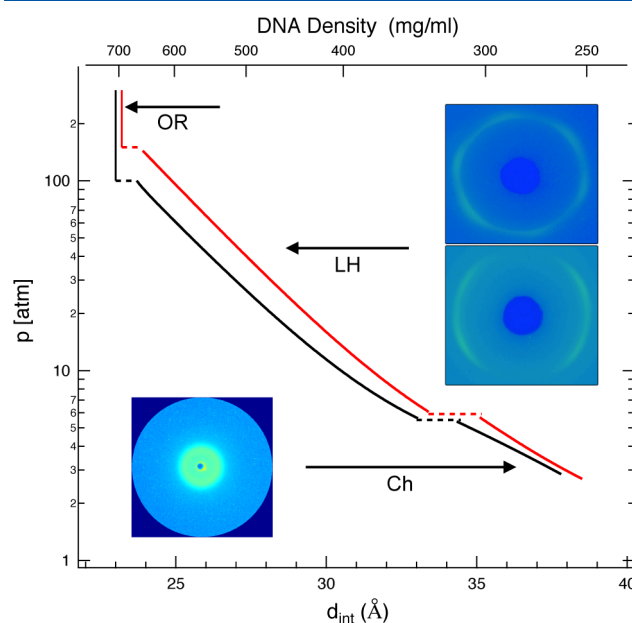


Figure 2. Equation of state for 0.5 M NaCl (upper curve - red) and 0.5 M LiCl (lower curve - black) fitted from the data. Lower horizontal axis is for interaxial spacings and upper horizontal axis is for DNA density, assuming hexagonal packing symmetry. At high densities, there is the OR → LH and, at lower densities, the LH → Ch phase transition. The curves are obtained from fits to osmotic stress raw data.³⁷ The images indicate the scattering intensity footprints of different phases. OR phase is virtually incompressible.

pressure, while changing the valency of the ion results in qualitative changes in the DNA–DNA interactions, phase diagram as well as EOS of DNA solutions.⁵²

Line Hexatic Phase. Here, the osmotic pressure can be decomposed into an electrostatic⁵³ and a hydration contribution:⁵⁴

$$p_0 = p_e + p_h \quad (2)$$

Both of them decay approximately exponentially with the interaxial spacing d_{int} . A simplified cell model and a linearized PB theory,⁵⁵ considering DNA as a charged cylinder of radius a

$\approx 10 \text{ \AA}$ for B-DNA, surrounded by electrolyte in a cylindrical cell of radius $R = d_{\text{int}}/2 = R(\rho)$, gives the electrostatic part of the osmotic pressure to the leading order as

$$p_e(R) = A_e \left[\frac{K_0(R/\lambda_D)}{K_1(a/\lambda_D)} \right]^2 \quad (3)$$

$K_0(x)$ and $K_1(x)$ are the cylindrical Bessel functions of the second kind. λ_D is the Debye length and $A_e = \sigma^2/\epsilon\epsilon_0$, where σ is the effective surface charge density of DNA, with ϵ_0 the vacuum permittivity and $\epsilon \approx 80$ for water. For fully charged B-DNA, $\sigma = e_0/(2\pi ab)$, where e_0 is the elementary charge and $b \approx 1.7 \text{ \AA}$ is the linear density of phosphates along the molecule. The Debye decay length can be obtained as $\lambda_D = 3.08 \text{ \AA} / \sqrt{I(M)}$, where $I(M)$ is the molar ionic concentration.

The short-range hydration repulsion contribution, $p_h(R)$, can be described phenomenologically by analogous formalism as the electrostatic repulsion⁵⁶ with

$$p_h(R) = A_h \left[\frac{K_0(R/\lambda_h)}{K_1(a/\lambda_h)} \right]^2 \quad (4)$$

with $\lambda_h \approx 2.2 \text{ \AA}$. Fits give $A_h = 1019 \text{ atm}$ and $A_e \approx 155 \text{ atm}$, independent of $[\text{NaCl}]$. The decomposition of the total osmotic pressure into electrostatic and hydration parts can be substantiated by a comprehensive theoretical description taking into account the details of the DNA–DNA interactions.^{57,58}

Cholesteric Phase. Short range positional order leads to strong fluctuation effects in this phase.^{59,60} They can be quantified via the steric Odijk deflection length or more appropriately through the fluctuation renormalized bare interaction potentials of the electrostatic and hydration types.^{13,61,62} The osmotic pressure in this case is given by

$$p_0 = p_e + p_h + p_{\text{fl}}(p_e + p_h) \quad (5)$$

indicating that the fluctuation part of the pressure p_{fl} depends on the underlying bare interaction part, $p_e + p_h$ and can be calculated directly from Frank–Oseen elastic free energy for polymer nematics⁶³ by tracing out the Gaussian fluctuations around a straight ground state.¹³ Osmotic pressure due to fluctuations is then derived as

$$p_{\text{fl}}(R) = k_B T (q_{\text{max}})^{5/2} \left[\frac{R^2}{20\pi \times 2^{3/2}} \left(\frac{B_b}{K} \right)^{1/4} \right] \times \left(-(\pi R^2) \frac{\partial \log B_b}{\partial (\pi R^2)} \right) \quad (6)$$

with where B_b is the bare osmotic compressibility modulus in the DNA cholesteric phase, i.e.

$$B_b = -(\pi R^2) \frac{\partial (p_e + p_h)}{\partial (\pi R^2)} \quad (7)$$

K is the bending elastic constant $K = \rho^{(2)} K_c$, where $\rho^{(2)}$ is the 2D number density of DNA chains perpendicular to their helical axes and $K_c = (k_B T) L_p$ is the bending rigidity of a single DNA chain, L_p ($\approx 50 \text{ nm}$ for B-DNA), depending very weakly on $[\text{NaCl}]$.^{64,65} q_{max} equals up to a constant (c) the Brillouin zone (per DNA chain) radius, i.e., $q_{\text{max}} \rightarrow c \times (\pi/d_{\text{int}})$, indicating that d_{int} can be replaced with an effective separation, $d_{\text{eff}} = d_{\text{int}}/c$. The fluctuation contribution in the stiffer LH phase was assumed to be negligible.¹³

The form of the entropic (i.e., fluctuational) contribution to the EOS immediately reveals that any bare osmotic pressure component with an exponential dependence on R , and a characteristic decay length λ is renormalized into a longer range form with a fluctuation-enhanced effective decay length $\sim 4\lambda$, due to the fourth root in p_{fl}^* , eq 6. This fluctuation enhancement of the underlying bare interactions is closely related to the behavior of interacting fluid membranes.^{66,67}

3. Line Hexatic - Cholesteric Phase Transition. At the Ch \rightarrow LH transition there is a discontinuous change of interaxial spacing from $d_{\text{int},C}^*$ to $d_{\text{int},H}^*$ at the transition osmotic pressure p_{tr} , resulting from the balance between the osmotic pressure in the LH and the Ch phases and an attractive osmotic pressure component, Π_{ea} , similar to the case of the van der Waals isotherm.⁴⁶ This effective attraction appears and can be interpreted also as a diminished repulsion emerging from a structural adaptation of the DNA chains to hydration interactions at high densities.⁵⁸ It is assumed to follow the same form as the bare interaction repulsion, i.e., the sum of two terms accounting for the two interactions of different origin, but with different characteristic decay lengths

$$\tilde{p}_{\text{ea}}(R) = -\tilde{A}_h \left[\frac{K_0(R/\tilde{\lambda}_h)}{K_1(a/\tilde{\lambda}_h)} \right]^2 - \tilde{A}_e \left[\frac{K_0(R/\tilde{\lambda}_e)}{K_1(a/\tilde{\lambda}_e)} \right]^2 \quad (8)$$

where $\tilde{\lambda}_h$ and $\tilde{\lambda}_e$ are found to be $\tilde{\lambda}_h \sim 2.4 \lambda_h$ and $\tilde{\lambda}_e \sim 2.4 \lambda_D$, respectively.³⁷

The fact that the effective attractive (diminished repulsion) osmotic pressure component has a decay length about two times larger than the repulsive yields a discontinuous first-order transition by the application of the standard Maxwell equal-area construction but otherwise does not qualitatively change the EOS. If the Ch \rightarrow LH transition starts at density ρ_1 and is complete at density ρ_2 , then the transition osmotic pressure is obtained from

$$\int_{\rho_1}^{\rho_2} \frac{d\rho}{\rho^2} (p(\rho) - p_{\text{tr}}) \equiv 0 \quad (9)$$

Fitting the experimental transition pressure, one then obtains the parameters of eq 8: $\tilde{A}_h \approx 14 \text{ atm}$ appears to be common for all salt concentrations, while \tilde{A}_e varies with salt concentration in the interval $[17\text{--}27] \text{ atm}$ for $[\text{NaCl}]$ between 0.1 and 0.4 M, respectively.

C. In Viro Equation of State. The inverse spool model, first proposed by Grosberg and collaborators^{68,69} and later repeatedly elaborated,^{32,70–81} is based on the idea of decomposition of the DNA free energy into an interaction term and a curvature term. The packing of DNA confined by the inner surface of the capsid in the inverse spool, allows it to act like a coiled osmotic spring once it is allowed to expand,⁸² ready to release its chemical and mechanical energy through the portal complex on docking onto a bacterial cell wall.⁸³

Elastic curvature energy is proportional to the square of local DNA curvature within the Euler–Kirchhoff model of an elastic filament,^{84–86} which appears to be a consistent description of DNA on mesoscales.^{84,87} The persistence length of DNA has been measured by a variety of methods, starting with light scattering,⁸⁸ with satisfactory consensus among the results.^{86,89} In the inverse spool decomposition, the interaction part of the inverse spool model is furthermore assumed to be given by the EOS of DNA in the bulk,³² as discussed above.

DNA conformation within the bacteriophage capsid can be treated in the framework of the *liquid crystalline nanodroplet*

model³² within a local thermodynamic theory based on the position dependent unit director $\mathbf{n} = \mathbf{n}(\mathbf{r})$ and density $\rho = \rho(\mathbf{r})$ fields.⁹⁰ This description consistently describes the complete local thermodynamic equilibrium, which seems experimentally well justified, except in the case of fast DNA ejection where nonequilibrium structures are possible and local thermodynamic equilibrium is not established. Assuming furthermore that the encapsidated DNA is in chemical equilibrium with the capsid exterior, the total free-energy density of thus encapsidated DNA can be decomposed as

$$f(\rho, \mathbf{n}, \nabla \mathbf{n}) = f_0(\rho(\mathbf{r})) + f_D(\rho(\mathbf{r}), \mathbf{n}(\mathbf{r}), \nabla \mathbf{n}(\mathbf{r})) - \rho(\mathbf{r})\mu \quad (10)$$

on the level of local thermodynamics.⁹¹ The first term represents the density dependent part of the free energy and describing the bulk DNA, while the second part is due to encapsidation induced elastic deformation, depending on the density as well as director. μ is the chemical potential associated with the equilibrium between the inside and the outside compartments. It is a function of the osmotic pressure in the external compartment. The index 0 will from now on be used solely for the bulk DNA that is not encapsidated and thus elastically deformed. Above, we do not specifically consider the issue of DNA chain connectivity (see below)^{93,94} and we note that the above *Ansatz* already takes into account the coupling between the thermal curvature fluctuations (entropic interactions¹¹), while the bending rigidity contains also the contribution of DNA–DNA interactions (bending rigidity renormalization⁹²).

At constant temperature the Gibbs–Duhem equation in the local thermodynamic approximation is reduced to

$$\frac{\partial p_0(\rho(\mathbf{r}))}{\partial \mu} = \rho(\mathbf{r}) \quad (11)$$

where $p_0(\rho)$ is the bulk EOS described in Section II B. Assuming furthermore that the deformation energy density is given by the Frank–Oseen *Ansatz*,^{95,96} one can write

$$f_D(\rho(\mathbf{r}), \mathbf{n}(\mathbf{r}), \nabla \mathbf{n}(\mathbf{r})) = \frac{1}{2} K_3 \rho(\mathbf{r}) (\mathbf{n}(\mathbf{r}) \times (\nabla \times \mathbf{n}(\mathbf{r})))^2 \quad (12)$$

The bending elastic modulus in the case of a semiflexible polymer liquid crystal has the form $K_3(\rho) \sim K_c L_{bp} \rho$ where $K_c = k_B T \mathcal{L}_p$ is the intrinsic elastic modulus of the polymer with \mathcal{L}_p its persistence length and L_{bp} is the phosphate-phosphate separation along the DNA. The other terms in the elastic free energy are assumed to be negligible: the splay term is neglected because the cylindrical spool *Ansatz* automatically satisfies the condition $\nabla \cdot \mathbf{n} = 0$, while the twist term is small on the length scale of a viral capsid.⁹⁷

First Integral. The thermodynamic equilibrium conditions are obtained from the Euler–Lagrange (EL) equations of the free energy eq 10. The first EL equation can be derived as^{95,96}

$$\frac{\partial}{\partial \rho} (f_0(\rho) + f_D(\rho, \mathbf{n}, \nabla \mathbf{n})) = \mu \quad (13)$$

and by introducing the stress tensor^{95,96}

$$\sigma_{ii}(\rho, \mathbf{n}, \nabla \mathbf{n}) = -\frac{\partial}{\partial (\partial n_k)} f_D(\rho, \mathbf{n}, \nabla \mathbf{n}) \partial_i n_k \quad (14)$$

the second EL equation can be written in the form

$$\rho \partial_i \mu_0(\rho) + \partial_i (\sigma_{ii}(\rho, \mathbf{n}, \nabla \mathbf{n})) = 0 \quad (15)$$

that describes the mechanical, i.e. force equilibrium in the system under osmotic stress. The forces originate partially in osmotic stresses stemming from the DNA–DNA interactions, the first term in the above equation, and partially in elastic stresses, the second term in the same equation.

These equations are the explicit thermodynamic equilibrium conditions that determine $\rho(\mathbf{r})$ and $\mathbf{n}(\mathbf{r})$ ^{95,96} and have a first integral in the form³²

$$p_0(\rho(\mathbf{r})) + f_D(\rho(\mathbf{r}), \mathbf{n}(\mathbf{r}), \nabla \mathbf{n}(\mathbf{r})) = p \quad (16)$$

where p is a constant, equal to external osmotic pressure if DNA is in equilibrium with the external phase, or equal to the osmotic pressure in the capsid, if it is not. The above first integral can be derived exactly for a nonuniform polymer nematic, i.e. $\mathbf{n} = \mathbf{n}(\mathbf{r})$ as well as $\rho = \rho(\mathbf{r})$, and is an extension of the standard result valid for a uniform nematic, $\rho = \text{const.}$ ^{95,96} The form of the first integral eq 16 is very similar to the first integral of the Poisson–Boltzmann theory where p_0 plays the role of van't Hoff pressure of ions and f_D the role of the Maxwell stress tensor.⁹⁸

In the local thermodynamic approximation $p_0(\rho(\mathbf{r}))$ is given simply by the bulk EOS eq 1 at the local DNA density equal to $\rho(\mathbf{r})$

$$p_0(\rho(\mathbf{r})) = p_0(\rho(\mathbf{r}); T, n_i) \quad (17)$$

The mechanical equilibrium condition eq 16 then simply demands that the full osmotic pressure p of encapsidated DNA is shared between the bulk equation of state and the deformation stress. The first integral eq 16 allows us to use the experimental EOS data directly, without any need to fit them to the corresponding free energies.^{70–77}

Inverse Spool and Generalizations. In the case of the inverse spool model with assumed cylindrical symmetry,³² the director has only a polar component with respect to the z axis, $\mathbf{n} = \hat{\phi}$, with

$$\mathbf{n} \times (\nabla \times \mathbf{n}) = \frac{\cos \theta}{r \sin \theta} \hat{\phi} + \frac{1}{r} \hat{r} \quad (18)$$

where $\hat{r}, \hat{\phi}$ and $\hat{\theta}$ are the unit radial, polar, and azimuthal vectors in polar spherical coordinates.⁹⁹ As a consequence the DNA density within the capsid has the form $\rho(\mathbf{r}) = \rho(r, \theta)$. For this director spatial profile, the mechanical equilibrium condition eq 16 assumes the form

$$p_0(\rho(r, \theta)) \left(1 + \frac{1}{2} \Phi(\rho(r, \theta))^{-1} \frac{\mathcal{L}_p L_{bp}}{r_{\perp}^2} \right) = p \quad (19)$$

where the osmotic coefficient is $\Phi(\rho(r, \theta)) = p_0(\rho(r, \theta)) / (k_B T \rho(r, \theta))$ and the axial distance from the inverse spool axis $r_{\perp} = r \sin \theta$. As is evident from the above equation, since for DNA solutions $\Phi \gg 1$, the effect of the curvature is overall small, relevant only around the axis of the spool at separation on the order of the geometric average of \mathcal{L}_p and L_{bp} scaled down by the osmotic coefficient. This sets also the size of a depletion hole of the DNA liquid crystalline nanodrop within the capsid.³²

Since the length of DNA inside the capsid, L , is fixed, one needs to add a constraint

$$L = L_{bp} 2\pi \int_0^{\pi} \sin \theta d\theta \int_0^R \rho(r, \theta) r^2 dr \quad (20)$$

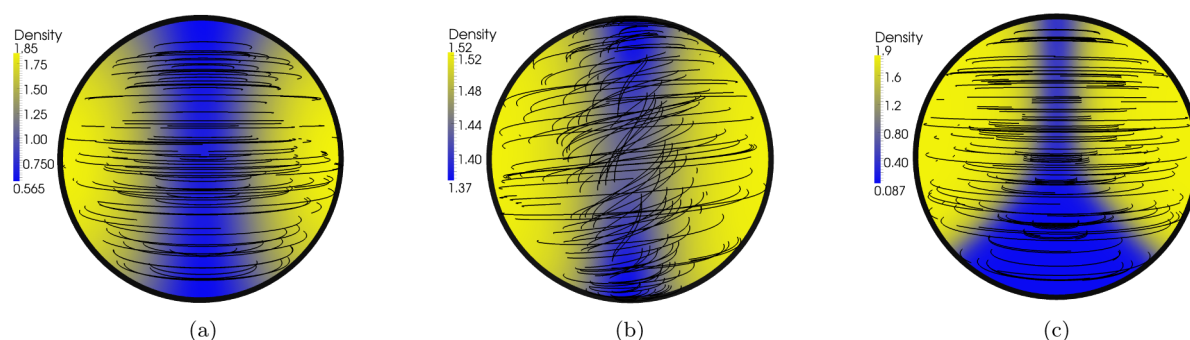


Figure 3. Density (represented by color coding, in arbitrary units) and orientation (represented by coarse-grained director lines) profiles obtained from the complete Landau–de Gennes free energy together with the imposed chain flux continuity constrained for main chain polymer nematics such as DNA.³⁴ (a) An almost ideal, spontaneous (no *Ansatz*) monophasic inverse spool configuration with disordered core. (b) Deviations from the inverse spool configuration with disordered core in phase equilibrium with the nematic periphery. In this quasi twisted-solenoid configuration occurring for more expensive density variations, director distortion in the core is reduced by spontaneous twisting of either sign (no chiral interaction is included in the free energy). (c) In the case of a wider confinement and cheaper density variations, nematic interactions and the chain flux constraint lead to broken polar symmetry with an asymmetric disordered core. The capsid is indicated by the black circular line.

A good approximate form of the density profile $\rho(r, \theta)$, obtained from eq 19 can be written in the form

$$\rho(r, \theta) = \rho_0 \frac{r_{\perp}^2}{r_{\perp}^2 + \xi^2} \quad (21)$$

where ρ_0 is the solution of the bulk EOS at pressure p

$$p_0(\rho_0) = p \quad (22)$$

and the size of the depletion hole, ξ , is given by

$$\xi^2 = \frac{1}{2} \Phi(\rho_0, p)^{-1} \mathcal{L}_p L_{bp} \quad (23)$$

where the osmotic coefficient is now $\Phi(\rho_0, p) = p/(k_B T \rho_0)$, to match the exact limits obtainable from eq 19. In general, the first integral equation can be solved numerically for $\rho(r, \theta)$ by using the EOS $p_0(\rho(r, \theta))$ described in the previous section.³² DNA bending has an important influence on the density profile within the capsid, with a clearly discernible cylindrical depletion hole of radius ξ , observable only for sufficiently low osmotic pressures (small genome packing fractions) where the inverse osmotic coefficient does not vanish. For high enough pressures, the capsid is almost uniformly filled with DNA.

Depending on whether DNA can exchange between the capsid compartment and the external solution, the total osmotic pressure p in the first integral eq 16 can be read in two different ways, depending on the context. If the length of the encapsidated DNA, eq 20, is given, then eq 19 provides a solution $\rho(r, \theta)$ as well as p , equilibrium pressure acting on the walls of the capsid. In this case eq 20, with the *Ansatz* eq 21, can be rewritten as

$$L = L(R, \rho_0(p), \Phi(\rho_0, p)) = L(R, p) \quad \rightarrow \quad p = p(L, R) \quad (24)$$

and the osmotic pressure within the capsid as a function of the encapsidated length can be read off directly. On the other hand, if the external osmotic pressure p is given and DNA is in equilibrium with the external solution at that osmotic pressure, then eq 20 provides the length of the encapsidated DNA, corresponding to that externally set osmotic pressure p .¹⁰⁰ The two problems then yield either $p = p(L, R)$ or $L = L(p, R)$.³² It is this latter case that is relevant for experiments started in the Gelbart lab and recently reviewed in ref 101.

The inverse spool *Ansatz* need not enter the description of DNA ordering *a priori*. A continuum description^{102,103} based on a minimal³³ or a full Landau–de Gennes free-energy model with the continuity of the DNA chain properly taken into account^{34,35} leads to more complicated and less symmetric packaging configurations, such as the folded toroid configuration as observed in experiments¹⁰⁴ and simulations;¹⁰⁵ in fact, the chain connectivity is particularly important in all the cases when no *a priori Ansatz* for the symmetry of the chain packing is introduced. In the coarse-grained, continuum description, the connectivity is taken into account by a constraint on the chain flux vector, linking the density variations and the director deformations, enforced by a penalty potential as described in ref 34. A simplified form of this constraint can be cast into the form of a divergence of a chain flux vector^{106–109}

$$\nabla \cdot (\rho_s \mathbf{n}) = 0 \quad (25)$$

where $\rho_s(\mathbf{r})$ is the surface density of polymer chains perforating the plane perpendicular to the nematic director $\mathbf{n}(\mathbf{r})$. In the minimal free-energy model, the chain flux is treated as a coarse-grained order parameter field, leading in general to nonaxially symmetric packaging topologies: the coaxial spool, the simple solenoid, and the twisted-solenoid, where only the twisted-solenoid can effectively fill the volume without the presence of voids.³³ The minimal free-energy model of Shin and Grason³³ can be generalized first of all by introducing the chain flux conservation law,³⁴ and splitting the free-energy into an elastic part containing Frank terms for splay, twist, and bend of the director, possibly with cholesteric interactions included³⁵ together with the polymer density part that selects two different densities corresponding to two different ordered phases, e.g., the line hexatic and the cholesteric phases, or the ordered and the isotropic phases. The chain flux continuity condition belongs to a hierarchy of conditions on the order parameters of different tensorial order of polymer nematogens;⁹³ the lowest order form of this hierarchy was derived by de Gennes¹⁰⁶ and Meyer.¹⁰⁷ The appropriate variables in this case are the complete director field, $\mathbf{a}(\mathbf{r})$, describing the orientation and the degree of order and defined as $\mathbf{a} = a\mathbf{n}$, where a is the degree of order with a maximum possible value of $a = 1$, and the polymer density field, $\rho(\mathbf{r})$, with the corresponding free-energy as³⁴

$$\tilde{f}(\rho, \mathbf{a}, \nabla \mathbf{a}) = \tilde{f}_0(\rho(\mathbf{r})) + \tilde{f}_D(\rho(\mathbf{r}), \mathbf{a}(\mathbf{r}), \nabla \mathbf{a}(\mathbf{r})) - \rho(\mathbf{r})\mu \quad (26)$$

The deformation energy, \tilde{f}_D , now contains all Frank terms, splay, twist, and bend, as well as their coupling to the density, whereas the bulk free-energy, $\tilde{f}_0(\rho(\mathbf{r}))$, contains the proper description of the density change for the different phase(s). Furthermore, the chain flux conservation is absolutely crucial and eliminates the redundant antipodal radial defects that would otherwise be present. The assumed boundary condition is that the orientation of the chain is tangential at the boundary, consistent also with the connectivity constraint.

These generalizations lead to even less symmetric thermodynamically stable packings, taking the place of the inverse spool ordering.^{34,35} In the case of no explicit inverse spool symmetry requirement, Figure 3 shows the inverse spool as well as packings of lesser symmetry that form if no specific *Ansatz* for director configurations is assumed. In fact, as we will see later, this trend can eventually lead to configurations of no explicit symmetry.

D. In Vitro vs In Viro. The existence of two mesophase transitions in bulk DNA, OR \rightarrow LH and LH \rightarrow Ch in addition to Ch \rightarrow I transition, see Figure 2, coupled with the first integral for encapsidated DNA for an inverse spool configuration, brings forth interesting consequences for the spatial organization of the viral genome. Disregarding the LH \rightarrow OR transition, limited anyhow to extremely high DNA densities, we remain with the first-order LH \rightarrow Ch and Ch \rightarrow I. Let us assume that the former one corresponds to an osmotic pressure p_{tr} , eq 9, equal to 6 atm for long Na-DNA, see Figure 2. The existence of a phase transition, with a possible coexistence of the two phases, then leads to two possible scenarios within the inverse spool model, as is clear from eq 19: either the largest total osmotic pressure in the capsid is below or above the transition osmotic pressure. In the former case

$$p_{tr} \geq p - \frac{1}{2}k_B T \rho_0(p) \frac{\mathcal{L}_p \mathcal{L}_{bp}}{R^2},$$

where $\rho_0(p)$ is approximately given by the solution of $p_0(\rho_0) = p$ with R the radius of the capsid, the encapsidated DNA inside the whole capsid is homogeneous in the Ch phase. In the latter case, with

$$p_{tr} \leq p - \frac{1}{2}k_B T \rho_0(p) \frac{\mathcal{L}_p \mathcal{L}_{bp}}{R^2},$$

there exists a critical radial distance from the inverse spool axis r_{\perp}^c , given approximately as

$$r_{\perp}^c{}^2 = \frac{2(p - p_{tr})}{k_B T \rho_0(p)} \mathcal{L}_p \mathcal{L}_{bp} \quad (27)$$

and a phase coexistence between the LH and Ch (or Ch and I) phases is indeed possible. Then the encapsidated DNA is not ordered homogeneously but is partly in the high density (LH) and partly in the low density (Ch) phase as shown in Figure 4. Should there be more phases between the Ch and the OR phase, there could be more coexistence regions within the capsid (see Discussion). There are indeed strong indications that DNA in the process of ejection could go through a sequence of ordered phases.^{110,111} In these estimates, we assumed that the free energies of both phases in equilibrium are given by the same expression corresponding to the deformation energy, eq 12. This is in general not the case, and a full Landau–de Gennes form of the free-energy, \tilde{f} , should be taken into consideration consistently.^{33–35}

The second case above is of course the more interesting one as it allows for a two(multiple in general)-phase equilibrium of encapsidated DNA. Assuming that DNA exhibits only LH and

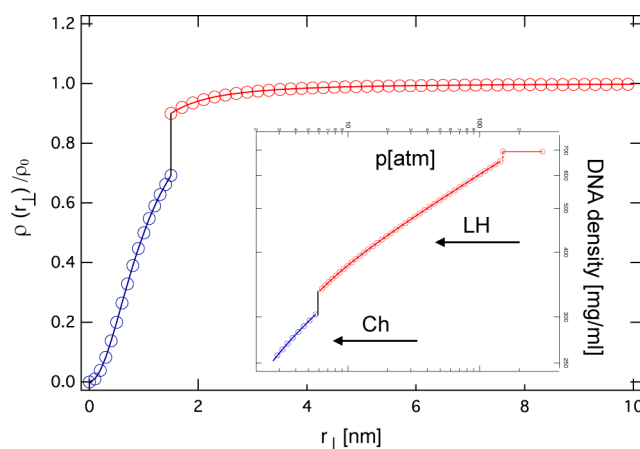


Figure 4. Equatorial (perpendicular to the inverse spool axis) normalized density profile as a function of the distance from the inverse spool axis (r_{\perp}). The inset shows the bulk EOS for 0.5 M NaCl, taken from Figure 2 but with interchanged axes. The bulk Ch \rightarrow LH transition is then converted into a phase boundary showing a discontinuity in the radial dependence of the DNA density $\rho(r_{\perp})$. ρ_0 is the value of the density at the capsid wall. Capsid radius was chosen as $R = 10$ nm, and the length of DNA was taken as $15 \mu\text{m}$.

Ch phases in the relevant regime of densities, see section II B, there thus exists a phase boundary between these phases within the capsid, indicated by a black vertical line in Figure 4, that has the same assumed cylindrical symmetry as the density distribution and the director of the encapsidated DNA. The phase boundary is characterized by a discontinuous change in the density, identical to the one observed in the bulk. The nature of the phase diagram of DNA in the bulk thus has immediate repercussions for the phase equilibria of encapsidated DNA, splitting the inverse spool into two single-phase regions.

However, the inverse spool *Ansatz* does not adequately describe the conformation of encapsidated DNA in general. Using the full Landau–de Gennes form of the nematic free-energy density^{33–35} $\tilde{f}(\rho, \mathbf{a}, \nabla \mathbf{a})$, eq 26, one can derive more general encapsidated configurations that are possibly devoid of any cylindrical symmetry and are of the general type observed also in simulations.^{105,112} Because in this case the configuration of the director and density fields can be quite complicated once one incorporates the effects of the actual symmetry of the capsid, as opposed to the idealized sphere, the coexistence surface can partition the interior of the capsid in multiple phase regions of the type observed recently by Leforestier et al.^{30,31} in cryomicroscopy of the T5 bacteriophage. This observation indicates that more complicated packing geometries can also be realized, such as cholesteric and line hexatic monodomains separated by phase coexistence walls, which in general do not conform to the inverse-spool paradigm.^{105,112}

Figure 5 shows a cross section through the encapsidated DNA density and director field configurations for the case where the deformation free energy is not given by the simplified Franck–Oseen elastic energy eq 12 and the inverse spool *Ansatz*, but it is obtained from the full unconstrained minimization of the Landau–de Gennes free energy with the I \rightarrow Ch phase coexistence.³⁵ The free energy describes the first-order phase transition with a density jump, as well as the complete deformation free energy with cholesteric interaction included.³⁵ The corresponding director and density configuration is complicated and sometimes shows no discernible

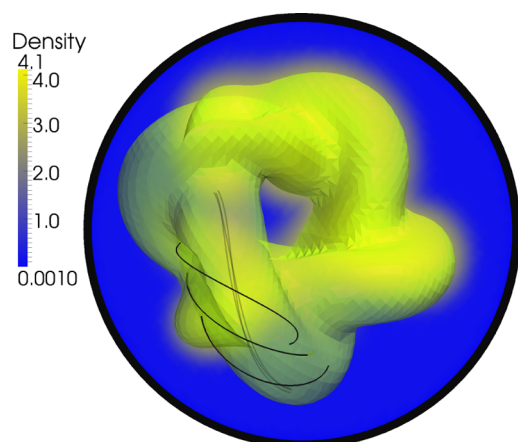


Figure 5. Equatorial cross section through the encapsidated DNA showing a complicated density and director configuration that does not display any evident inverse spool cylindrical symmetry. Characteristically, the director lines resemble a knot easily discernible by the iso-density surface. The director runs axially in the tube centers and twists around them due to chirality, such that the tubes meet compatibly and there are no defects. The Landau–de Gennes free energy includes the $I \rightarrow$ Ch phase coexistence as well as cholesteric terms in the elastic deformation free energy and the constraint of chain continuity. The orientation and density profiles result from a choice of different phenomenological parameters. For details, see ref 35. The capsid is indicated by the black circular line.

symmetry, see Figure 5, and could be described as a *phase mosaic* configuration.

III. DISCUSSION

The main lessons of the foregoing discussion are 2-fold. First, the behavior of encapsidated DNA mirrors closely the behavior of bulk DNA solutions at the same bathing conditions: temperature, type and concentration of salt, and osmotic pressure. The form of the EOS depends on the density of DNA and can be in fact written to the lowest order as a sum of terms decaying exponentially with interaxial separation with different decay lengths. At densities corresponding to the LH phase, between 350 and 650 mg/mL, the EOS is composed of the contribution of electrostatic and hydration interactions, with decay lengths equal to the Debye length and the hydration length, showing no entropic contributions due to very spatially constrained conformational fluctuations of the DNAs. In the Ch phase, extending below 350 mg/mL and then all the way to the isotropic phase setting in at 13 mg/mL, conformational fluctuations are pronounced and contribute essentially to the EOS, changing the nature of its dependence on the DNA density in a way to enhance the range of the underlying bare interactions, showing dominant entropic terms that decay with four times the Debye length and hydration length. The transition between the Ch and the LH phases, in the range of densities relevant also for the DNA encapsidation, is first-order and demonstrates the existence of structural adaptations of DNA helices to the stronger hydration and electrostatic interactions at larger densities.³⁷ Second, within a continuum nematic droplet model the bulk EOS part derived from osmotic stress measurements contains the full DNA–DNA interaction energy together with the confinement entropy as clearly pointed out by Ben-Shaul recently.⁷⁹ One can also derive that the effect of the deformation of the encapsidated DNA, as seen in the first integral of the equilibrium equations, is to introduce

another local curvature dependent term to the effective osmotic pressure. This in general modifies the total osmotic pressure of encapsidated DNA amplifying it in proportion to the elastic deformation free-energy density. Elastic stresses also allow for a coexistence of the Ch and LH phases within the capsid. Within the simple inverse spool model, the coexistence surface is cylindrical, but the model can be in general much more complicated when details of the capsid symmetry and molecular shape of its inner surface are taken into account.

Apart from the changes in the EOS wrought by the presence of condensing polyions that we did not discuss,³⁷ there are other details and additional features that we also did not explicitly take into consideration. The length of DNA profoundly changes the phase diagram of DNA. There are indications⁸ that for solutions of short 50 nm DNA fragments, apart from the Ch phase, the LH phase region actually decomposes into two (meso)phases: the 2D hexagonal columnar liquid crystalline phase, at densities in the range of 534–443 mg/mL, and the 3D hexagonal columnar crystalline phase, at densities in the range of 443–380 mg/mL. Different mesophases can then actually coexist in a T5 bacteriophage either spatially or temporally when it undergoes progressive ejection and the length of encapsidated DNA decreases.¹¹¹ In the language introduced above, we could say that there may be multiple coexistence surfaces within the encapsidated genome separating different mesophases at different densities. This would lead to *phase mosaic* as opposed to monophasic *inverse spool* configurations of the encapsidated genome with a complicated coexistence of different DNA (meso)phases within the capsid. Furthermore, the pronounced conformational fluctuations of DNA, which determine the EOS in the Ch phase in the bulk, will be suppressed by the capsid walls. A similar effect of boundary layer fluctuation suppression in lipid bilayers leads to the s.c. “vapor pressure paradox”.^{113,114}

The line of reasoning presented above depends on the continuum modelisation that could be of course subject to criticism and could be invalidated at a less coarse-grained level. While this criticism could be relevant, one should not gloss over different types of drawbacks of at first sight “exact” results provided by the simulation approach.^{115–118} The weakest part of the simulation studies are the assumed model forms of the complicated DNA–DNA interaction potentials that as a rule compare poorly with the measured interaction potentials.¹¹⁹ This is especially the case for the hydration interaction potentials, due to water structuring, which are not properly taken into account in any simulation. The question of molecular and atomic potentials is thus far from settled and could eventually invalidate all the interim results purporting to illuminate and surpass the obviously flawed continuum approach which can be expected to be qualitatively relevant, if not quantitatively predictive, in many contexts of the nanoscale science.¹²⁰

■ AUTHOR INFORMATION

Corresponding Author

*E-mail: rudolf.podgornik@ijs.si.

Notes

The authors declare no competing financial interest.

■ ACKNOWLEDGMENTS

This research was supported by the U.S. Department of Energy, Office of Basic Energy Sciences, Division of Materials Sciences

and Engineering under award DE-SC0008176. D.S. acknowledges the financial support of the Slovenian Research Agency (ARRS) under award J1-7435. We acknowledge the graphical input of L. Čurovič in preparing Figure 1.

REFERENCES

- (1) Livolant, F.; Leforestier, A. Condensed Phases of DNA: Structures and Phase Transitions. *Prog. Polym. Sci.* **1996**, *21*, 1115–1164.
- (2) Evdokimov, Y. M.; Salyanov, V. I.; Skuridin, S. G. *Nanostructures and Nanoconstructions based on DNA*; CRC Press: Boca Raton, FL, 2012.
- (3) Robinson, C. Liquid-Crystalline Structures in Polypeptide Solutions. *Tetrahedron* **1961**, *13*, 219–234.
- (4) Rill, R. L. Liquid Crystalline Phases in Concentrated Aqueous Solutions of Na⁺ DNA. *Proc. Natl. Acad. Sci. U. S. A.* **1986**, *83*, 342–346.
- (5) Strzelecka, T. E.; Davidson, M. E.; Rill, R. L. Multiple Liquid Crystal Phases of DNA at High Concentrations. *Nature* **1988**, *331*, 457–460.
- (6) Livolant, F.; Levelut, A. M.; Doucet, J.; Benoit, J. P. The Highly Concentrated Liquid-Crystalline Phase of DNA Is Columnar Hexagonal. *Nature* **1989**, *339*, 724–726.
- (7) Livolant, F. Ordered Phases of DNA in Vivo and in Vitro. *Phys. A* **1991**, *176*, 117–137.
- (8) Durand, D.; Doucet, J.; Livolant, F. A Study of the Structure of Highly Concentrated Phases of DNA By X-Ray Diffraction. *J. Phys. II* **1992**, *2*, 1769–1783.
- (9) Nakata, M.; Zanchetta, G.; Chapman, B. D.; Jones, C. D.; Cross, J. O.; Pindak, R.; Bellini, T.; Clark, N. A. End-to-End Stacking and Liquid Crystal Condensation of 6-to-20-Base Pair DNA Duplexes. *Science* **2007**, *318*, 1276–1279.
- (10) Rau, D. C.; Lee, B. K.; Parsegian, V. A. Measurement of the Repulsive Force Between Polyelectrolyte Molecules in Ionic Solution: Hydration Forces Between Parallel DNA Double Helices. *Proc. Natl. Acad. Sci. U. S. A.* **1984**, *81*, 2621–2625.
- (11) Podgornik, R.; Rau, D. C.; Parsegian, V. A. The Action of Interhelical Forces on the Organization of DNA Double Helices: Fluctuation-Enhanced Decay of Electrostatic Double Layer and Hydration Forces. *Macromolecules* **1989**, *22*, 1780–1786.
- (12) Podgornik, R.; Strey, H. H.; Gawrisch, K.; Rau, D. C.; Rupprecht, A.; Parsegian, V. A. Bond Orientational Order, Molecular Motion, and Free Energy of High-Density DNA Mesophases. *Proc. Natl. Acad. Sci. U. S. A.* **1996**, *93*, 4261–4266.
- (13) Strey, H. H.; Parsegian, V. A.; Podgornik, R. Equation of State For Polymer Liquid Crystals: Theory and Experiment. *Phys. Rev. E: Stat. Phys., Plasmas, Fluids, Relat. Interdiscip. Top.* **1999**, *59*, 999–1008.
- (14) Earnshaw, W. C.; King, J.; Harrison, S. C.; Eiserling, F. A. The Structural Organization of DNA Packaged Within the Heads of T4 Wild-Type, Isometric and Giant Bacteriophages. *Cell* **1978**, *14*, 559–568.
- (15) We use the term *in viro* as a shorthand that refers to the behavior of the genome inside the capsid.
- (16) Cerritelli, M. E.; Cheng, N.; Rosenberg, A. H.; McPherson, C. E.; Booy, F. P.; Steven, A. C. Encapsidated Conformation of Bacteriophage T7 DNA. *Cell* **1997**, *91*, 271–280.
- (17) Fokine, A.; Chipman, P. R.; Leiman, P. G.; Mesyanzhinov, V. V.; Rao, V. B.; Rossmann, M. G. Molecular Architecture of the Prolate Head of Bacteriophage T4. *Proc. Natl. Acad. Sci. U. S. A.* **2004**, *101*, 6003–6008.
- (18) Xiang, Y.; Morais, M. C.; Battisti, A. J.; Grimes, S.; Jardine, P. J.; Anderson, D. L.; Rossmann, M. G. Structural Changes of Bacteriophage Phi29 Upon DNA Packaging and Release. *EMBO J.* **2006**, *25*, 5229–5239.
- (19) Chang, J.; Weigele, P.; King, J.; Chiu, W.; Jiang, W. Cryo-EM Asymmetric Reconstruction of Bacteriophage P22 Reveals Organization of Its DNA Packaging and Infecting Machinery. *Structure* **2006**, *14*, 1073–1082.
- (20) Jiang, W.; Chang, J.; Jakana, J.; Weigele, P.; King, J.; Chiu, W. Structure of Epsilon15 Bacteriophage Reveals Genome Organization and DNA Packaging/Injection Apparatus. *Nature* **2006**, *439*, 612–616.
- (21) Roos, W. H.; Bruinsma, R.; Wuite, G. J. L. Physical Virology. *Nat. Phys.* **2010**, *6*, 733–743.
- (22) Knobler, C. M.; Gelbart, W. M. Physical Chemistry of DNA Viruses. *Annu. Rev. Phys. Chem.* **2009**, *60*, 367–383.
- (23) Keller, N.; del Toro, D.; Grimes, S.; Jardine, P. J.; Smith, D. E. Repulsive DNA-DNA Interactions Accelerate Viral DNA Packaging in Phage Phi29. *Phys. Rev. Lett.* **2014**, *112*, 248101–248105.
- (24) Leforestier, A.; Livolant, F. The Bacteriophage Genome Undergoes a Succession of Intracapsid Phase Transitions Upon DNA Ejection. *J. Mol. Biol.* **2010**, *396*, 384–395.
- (25) Lemay, S. G.; Panja, D.; Molineux, I. J. Role of Osmotic and Hydrostatic Pressures in Bacteriophage Genome Ejection. *Phys. Rev. E* **2013**, *87*, 022714–022718.
- (26) Podgornik, R.; Harries, D.; DeRouchey, J.; Strey, H. H.; Parsegian, V. A. Interactions in Macromolecular Complexes Used As Nonviral Vectors For Gene Delivery. In *Gene Therapy: Therapeutic Mechanisms and Strategies*; Smyth Templeton, N., Ed.; Marcel Dekker: New York, 2008.
- (27) Petrov, A. S.; Lim-Hing, C.; Harvey, S. C. Packaging of DNA By Bacteriophage Epsilon15: Structure, Forces, and Thermodynamics. *Structure* **2007**, *15*, 807–812.
- (28) Petrov, A. S.; Harvey, S. C. Structural and Thermodynamic Principles of Viral Packaging. *Structure* **2007**, *15*, 21–27.
- (29) Comolli, L. R.; Spakowitz, A. J.; Siegerist, C. E.; Jardine, P. J.; Grimes, S.; Anderson, D. L.; Bustamante, C.; Downing, K. H. Three-Dimensional Architecture of the Bacteriophage Phi29 Packaged Genome and Elucidation of Its packaging process. *Virology* **2008**, *371*, 267–277.
- (30) Leforestier, A.; Brasiles, S.; de Frutos, M.; Raspaud, E.; Letellier, L.; Tavares, P.; Livolant, F. Bacteriophage T5 DNA Ejection Under Pressure. *J. Mol. Biol.* **2008**, *384*, 730–739.
- (31) Leforestier, A.; Livolant, F. The Bacteriophage Genome Undergoes a Succession of Intracapsid Phase Transitions Upon DNA Ejection. *J. Mol. Biol.* **2010**, *396*, 384–395.
- (32) Šiber, A.; Dragar, M.; Parsegian, V. A.; Podgornik, R. Packing Nanomechanics of Viral Genomes. *Eur. Phys. J. E: Soft Matter Biol. Phys.* **2008**, *26*, 317–325.
- (33) Shin, H.; Grason, G. M. Filling the Void in Confined Polymer Nematics: Phase Transitions in a Minimal Model of dsDNA Packing. *EPL* **2011**, *96*, 36007–36013.
- (34) Svenšek, D.; Veble, G.; Podgornik, R. Confined Nematic Polymers: Order and Packing in a Nematic Drop. *Phys. Rev. E* **2010**, *82*, 011708–011721.
- (35) Svenšek, D.; Podgornik, R. Confined Chiral Polymer Nematics: Ordering and Spontaneous Condensation. *EPL* **2012**, *100*, 66005–66011.
- (36) Podgornik, R.; Strey, H. H.; Parsegian, V. A. Colloidal DNA. *Curr. Opin. Colloid Interface Sci.* **1998**, *3*, 534–539.
- (37) Yasar, S.; Podgornik, R.; Valle-Orero, J.; Johnson, M. R.; Parsegian, V. A. Continuity of States Between the Cholesteric → Line Hexatic Transition and the Condensation Transition in DNA Solutions. *Sci. Rep.* **2014**, *4*, 6877–6886.
- (38) Lindsay, S. M.; Lee, S. M.; Powell, J. W.; Weidlich, T.; Demarco, C.; Lewen, G. D.; Tao, N. J.; Rupprecht, A. The Origin of A To B Transition in DNA Fibers and Films. *Biopolymers* **1988**, *27*, 1015–1043.
- (39) Parsegian, V. A.; Rand, R. P.; Fuller, N. L.; Rau, D. C. Osmotic Stress for the Direct Measurement of Intermolecular Forces. *Methods Enzymol.* **1986**, *127*, 400–416.
- (40) Stanley, C. B.; Strey, H. H. Measuring Osmotic Pressure of Poly(Ethylene Glycol) Solutions By Sedimentation Equilibrium Ultracentrifugation. *Macromolecules* **2003**, *36*, 6888–6893.
- (41) Beck, R.; Deek, J.; Jones, J. B.; Safinya, C. R. Gel-Expanded To Gel-Condensed Transition in Neurofilament Networks Revealed By Direct Force Measurements. *Nat. Mater.* **2010**, *9*, 40–46.

- (42) Toner, J. Bond-Orientationally-Ordered Phases That Scatter Light Strongly. *Phys. Rev. A: At., Mol., Opt. Phys.* **1983**, *27*, 1157–1163.
- (43) Strey, H. H.; Wang, J.; Podgornik, R.; Rupperecht, A.; Yu, L.; Parsegian, V. A.; Sirota, E. B. Refusing To Twist: Demonstration of a Line Hexatic Phase in DNA Liquid Crystals. *Phys. Rev. Lett.* **2000**, *84*, 3105–3108.
- (44) Leforestier, A.; Livolant, F. Supramolecular Ordering of DNA in the Cholesteric Liquid Crystalline Phase: an Ultrastructural Study. *Biophys. J.* **1993**, *65*, 56–72.
- (45) Merchant, K.; Rill, R. L. DNA Length and Concentration Dependencies of Anisotropic Phase Transitions of DNA Solutions. *Biophys. J.* **1997**, *73*, 3154–3163.
- (46) Chaikin, P. M.; Lubensky, T. C. *Principles of Condensed Matter Physics*; Cambridge University Press: Cambridge, 1995.
- (47) Nelson, D. R. Vortex Lattice Melts Like Ice. *Nature* **1995**, *375*, 356–357.
- (48) Bloomfield, V. A.; Crothers, D. M.; Tinoco, I. J. *Nucleic Acids. Structure, Properties and Functions*; University Science Books: Sausalito, CA, 2000.
- (49) Rau, D. C.; Parsegian, V. A. Direct Measurement of the Intermolecular Forces Between Counterion-Condensed DNA Double Helices. Evidence for Long-Range Attractive Hydration Forces. *Biophys. J.* **1992**, *61*, 246–259.
- (50) Strey, H. H.; Podgornik, R.; Parsegian, V. A. Colloidal DNA. *Curr. Opin. Colloid Interface Sci.* **1998**, *3*, 534–539.
- (51) Podgornik, R.; Rau, D. C.; Parsegian, V. A. Parametrization of Direct and Soft-undulatory Forces between DNA Double Helical Polyelectrolytes in Solutions of Several Different Anions and Cations. *Biophys. J.* **1994**, *66*, 962–971.
- (52) Lipfert, J.; Doniach, S.; Das, R.; Herschlag, D. Understanding Nucleic Acid-Ion Interactions. *Annu. Rev. Biochem.* **2014**, *83*, 813–841.
- (53) Gelbart, W. M.; Bruinsma, R.; Pincus, P. A.; Parsegian, V. A. DNA-Inspired Electrostatics. *Phys. Today* **2000**, *53*, 38–44.
- (54) Stanley, C.; Rau, D. C. Evidence for Water Structuring Forces Between Surfaces. *Curr. Opin. Colloid Interface Sci.* **2011**, *16*, 551–556.
- (55) Holm, C.; KŽkicheff, P.; Podgornik, R. Electrostatic Effects in Soft Matter and Biophysics. *Proceedings of the NATO Advanced Research Workshop on Electrostatic Effects in Soft Matter and Biophysics Les Houches*; Springer: Berlin, 2000.
- (56) Kanduč, M.; Schlaich, M.; Schneck, E.; Netz, R. R. Hydration Repulsion Between Membranes and Polar Surfaces: Simulation Approaches Versus Continuum Theories. *Adv. Colloid Interface Sci.* **2014**, *208*, 142–152.
- (57) Cherstvy, A. G. Electrostatic Interactions in Biological DNA-Related Systems. *Phys. Chem. Chem. Phys.* **2011**, *13*, 9942–9968.
- (58) Kornyshev, A. A.; Lee, D. J.; Leikin, S.; Wynveen, A. Structure and Interactions of Biological Helices. *Rev. Mod. Phys.* **2007**, *79*, 943–996.
- (59) Podgornik, R. Interactions and Conformational Fluctuations in DNA Arrays. In *Soft condensed matter physics in molecular and cell biology (Scottish graduate series)*; Poon, W. C. K., Andelman, D., Eds.; Taylor & Francis: New York, 2006.
- (60) Podgornik, R.; Parsegian, V. A. Molecular Fluctuations in the Packing of Polymeric Liquid-Crystals. *Macromolecules* **1990**, *23*, 2265–2269.
- (61) Podgornik, R.; Rau, D. C.; Parsegian, V. A. The Action of Interhelical Forces on the Organization of DNA Double Helices: Fluctuation-Enhanced Decay of Electrostatic Double Layer and Hydration Forces. *Macromolecules* **1989**, *22*, 1780–1786.
- (62) Lee, D. J.; Wynveen, A.; Kornyshev, A. A.; Leikin, S. Undulations Enhance the Effect of Helical Structure on DNA Interactions. *J. Phys. Chem. B* **2010**, *114*, 11668–11680.
- (63) Grason, G. M. Braided Bundles and Compact Coils: The Structure and Thermodynamics of Hexagonally Packed Chiral Filament Assemblies. *Phys. Rev. E* **2009**, *79*, 041919–041933.
- (64) Baumann, C. G.; Smith, S. B.; Bloomfield, V. A.; Bustamante, C. Ionic Effects on the Elasticity of Single DNA Molecules. *Proc. Natl. Acad. Sci. U. S. A.* **1997**, *94*, 6185–6190.
- (65) Tomić, S.; Vuletić, T.; Babić, S. D.; Krča, S.; Ivanković, D.; Griparić, T.; Podgornik, R. Screening and Fundamental Length Scales in Semidilute Na-DNA Aqueous Solutions. *Phys. Rev. Lett.* **2006**, *97*, 098303–098306.
- (66) Podgornik, R.; Parsegian, V. A. Thermal-Mechanical Fluctuations of Fluid Membranes in Confined Geometries: The Case of Soft Confinement. *Langmuir* **1992**, *8*, 557–562.
- (67) Lu, B. S.; Podgornik, R. Effective Interactions Between Fluid Membranes. *Phys. Rev. E* **2015**, *92*, 022112–022126.
- (68) Gabashvili, I. S.; Grosberg, A. Y.; Kuznetsov, D. V.; Mrevlishvili, G. M. Theoretical Model of the DNA Packaging in the Phage Head. *Biofizika* **1991**, *36*, 780–787.
- (69) Grosberg, A. Y.; Zhestkov, A. V. On the Theory of Packing of Double-Helical DNA: Globular State of Uniform Elastic Macromolecule in the Small Volume Cavity. *Biofizika* **1991**, *36*, 788–793.
- (70) Odijk, T. Hexagonally Packed DNA Within Bacteriophage T7 Stabilized by Curvature Stress. *Biophys. J.* **1998**, *75*, 1223–1227.
- (71) Odijk, T. Statics and Dynamics of Condensed DNA Within Phages and Globules. *Philos. Trans. R. Soc., A* **2004**, *362*, 1497–1517.
- (72) Kindt, J.; Tzllil, S.; Ben-Shaul, A.; Gelbart, W. M. DNA Packaging and Ejection Forces in Bacteriophage. *Proc. Natl. Acad. Sci. U. S. A.* **2001**, *98*, 13671–13674.
- (73) Purohit, N. K.; Kondev, J.; Phillips, R. Mechanics of DNA Packaging in Viruses. *Proc. Natl. Acad. Sci. U. S. A.* **2003**, *100*, 3173–3178.
- (74) Purohit, N. K.; Inamdar, M. M.; Grayson, P. D.; Squires, T. M.; Kondev, J.; Phillips, R. Forces During Bacteriophage DNA Packaging and Ejection. *Biophys. J.* **2005**, *88*, 851–866.
- (75) Tzllil, S.; Kindt, J. T.; Gelbart, W. M.; Ben-Shaul, A. Forces and Pressures in DNA Packaging and Release From Viral Capsids. *Biophys. J.* **2003**, *84*, 1616–1627.
- (76) Klug, W. S.; Feldmann, M. T.; Ortiz, M. Three-Dimensional Director-Field Predictions of Viral DNA Packing Arrangements. *Comput. Mech.* **2005**, *35*, 146–152.
- (77) Klug, W. S.; Ortiz, M. A Director-Field Model of DNA Packaging in Viral Capsids. *J. Mech. Phys. Solids* **2003**, *51*, 1815–1847.
- (78) Oskolkov, N. N.; Linse, P.; Potemkin, I. I.; Khokhlov, A. R. Nematic Ordering of Polymers in Confined Geometry Applied to DNA Packaging in Viral Capsids. *J. Phys. Chem. B* **2011**, *115*, 422–432.
- (79) Ben-Shaul, A. Reply to the Comment by S. Harvey On "Entropy, Energy, and Bending of DNA in Viral Capsids. *Biophys. J.* **2014**, *106*, 493–496.
- (80) Evilevitch, A.; Lavelle, L.; Knobler, C. M.; Raspud, E.; Gelbart, W. M. Osmotic Pressure Inhibition of DNA Ejection From Phage. *Proc. Natl. Acad. Sci. U. S. A.* **2003**, *100*, 9292–9295.
- (81) Purohit, P. K.; Inamdar, M. M.; Grayson, P. D.; Squires, T. M.; Kondev, J.; Phillips, R. Forces During Bacteriophage DNA Packaging and Ejection. *Biophys. J.* **2005**, *88*, 851–866.
- (82) Gelbart, W. M.; Knobler, C. M. The Physics of Phages. *Phys. Today* **2008**, *61*, 42–47.
- (83) Smith, D. E.; Tans, S. J.; Smith, S. B.; Grimes, S.; Anderson, D. L.; Bustamante, C. The Bacteriophage Straight ϕ 29 Portal Motor Can Package DNA Against a Large Internal Force. *Nature* **2001**, *413*, 748–752.
- (84) Wiggins, P. A.; van der Heijden, T.; Moreno-Herrero, F.; Spakowitz, A.; Phillips, R.; Widom, J.; Dekker, C.; Nelson, P. C. High Flexibility of DNA on Short Length Scales Probed by Atomic Force Microscopy. *Nat. Nanotechnol.* **2006**, *1*, 137–141.
- (85) Qu, H.; Tseng, C. Y.; Wang, Y.; Levine, A. J.; Zocchi, G. The Elastic Energy of Sharply Bent Nicked DNA. *Europhys. Lett.* **2010**, *90*, 18003–18007.
- (86) Vologodskii, A. *Biophysics of DNA*; Cambridge University Press: Cambridge, U.K., 2015.
- (87) Williams, M. C.; Rouzina, I. Force Spectroscopy of Single DNA and RNA Molecules. *Curr. Opin. Struct. Biol.* **2002**, *12*, 330–336.
- (88) Peterlin, A. Light Scattering by Very Stiff Chain Molecules. *Nature* **1953**, *171*, 259–260.

- (89) Hagerman, P. J. Flexibility of DNA. *Annu. Rev. Biophys. Biophys. Chem.* **1988**, *17*, 265–286.
- (90) Kulić, I. M.; Andrienko, D.; Deserno, M. Twist-Bend Instability for Toroidal DNA Condensates. *Europhys. Lett.* **2004**, *67*, 418–424.
- (91) Rowlinson, J. S.; Widom, B. *Molecular Theory of Capillarity*; Dover Publications: Dover, 2003.
- (92) Podgornik, R.; Hansen, P. L.; Parsegian, V. A. Elastic Moduli Renormalization in Self-Interacting Stretchable Polyelectrolytes. *J. Chem. Phys.* **2000**, *113*, 9343–9350.
- (93) Svenšek, D.; Grason, G. M.; Podgornik, R. Tensorial Conservation Law for Nematic Polymers. *Phys. Rev. E* **2013**, *88*, 052603–052609.
- (94) Svenšek, D.; Podgornik, R. Correlation Functions of Main-Chain Polymer Nematics Constrained by Tensorial and Vectorial Conservation Laws. *J. Chem. Phys.* **2015**, *143*, 114902–114914.
- (95) Kosevich, A. M.; Lifshitz, E. M.; Landau, L. D.; Pitaevskii, L. P. *Theory of Elasticity*, 3rd ed.; Butterworth-Heinemann: Oxford, U.K., 1986; Vol. 7.
- (96) de Gennes, P. G.; Prost, J. *The Physics of Liquid Crystals (International Series of Monographs on Physics)*; Oxford University Press: Oxford, U.K., 1995.
- (97) Strey, H. H.; Parsegian, V. A.; Podgornik, R. Equation of State for Polymer Liquid Crystals: Theory and Experiment. *Phys. Rev. E: Stat. Phys., Plasmas, Fluids, Relat. Interdiscip. Top.* **1999**, *59*, 999–1008.
- (98) Markovich, T.; Andelman, D.; Podgornik, R. Charged Membranes: Poisson-Boltzmann Theory, DLVO Paradigm and Beyond. In *Handbook of Lipid Membranes*; Safyria, C.; Raedler, J., Eds.; Taylor & Francis: New York, 2016; Chapter 9, pp 1–57.
- (99) Arfken, G. *Mathematical Methods for Physicists*; Academic Press: New York, 1985; pp 102–111.
- (100) Evilevitch, A.; Lavelle, L.; Knobler, C. M.; Raspaud, E.; Gelbart, W. M. Osmotic Pressure Inhibition of DNA Ejection From Phage. *Proc. Natl. Acad. Sci. U. S. A.* **2003**, *100*, 9292–9295.
- (101) Nurmemmedov, E.; Castelnovo, M.; Catalano, C. E.; Evilevitch, A. Biophysics of Viral Infectivity: Matching Genome Length With Capsid Size. *Q. Rev. Biophys.* **2007**, *40*, 327–356.
- (102) Klug, W. S.; Feldmann, M. T.; Ortiz, M. Three-Dimensional Director-Field Predictions of Viral DNA Packing Arrangements. *Comput. Mech.* **2005**, *35*, 146–152.
- (103) Arsuaga, J.; Tan, R. K. Z.; Vazquez, M.; Sumners, D. W.; Harvey, S. C. Investigation of Viral DNA Packaging Using Molecular Mechanics Models. *Biophys. Chem.* **2002**, *101-102*, 475–484.
- (104) Hud, N. V. Double-Stranded DNA Organization in Bacteriophage Heads: An Alternative Toroid-Based Model. *Biophys. J.* **1995**, *69*, 1355–1362.
- (105) Forrey, C.; Muthukumar, M. Langevin Dynamics Simulations of Genome Packing in Bacteriophage. *Biophys. J.* **2006**, *91*, 25–41.
- (106) de Gennes, P. G. Polymeric Liquid Crystals: Frank Elasticity and Light Scattering. *Mol. Cryst. Liq. Cryst.* **1976**, *34*, 177–182.
- (107) Meyer, R. Macroscopic Phenomena in Nematic Polymers In *Polymer Liquid Crystals*; Ciferri, A., Krigbaum, W. R., Meyer, R., Eds.; Academic Press: New York, 1982; pp 133–163.
- (108) Selinger, J. V.; Bruinsma, R. F. Hexagonal and Nematic Phases of Chains. I. Correlation functions. *Phys. Rev. A: At, Mol, Opt. Phys.* **1991**, *43*, 2910–2921.
- (109) Nelson, D. R. Line Liquids. *Phys. A* **1991**, *177*, 220–232.
- (110) Liu, T.; Sae-Ueng, U.; Li, D.; Lander, G. C.; Zuo, X.; Jönsson, B.; Rau, D. C.; Shefer, I.; Evilevitch, A. Solid-To-Fluid-Like DNA Transition in Viruses Facilitates Infection. *Proc. Natl. Acad. Sci. U. S. A.* **2014**, *111*, 14675–14680.
- (111) Leforestier, A.; Livolant, F. The Bacteriophage Genome Undergoes a Succession of Intra-Capsid Phase Transitions Upon DNA Ejection. *J. Mol. Biol.* **2010**, *396*, 384–395.
- (112) Petrov, A. S.; Harvey, S. C. Packaging Double-Helical DNA Into Viral Capsids: Structures, Forces, and Energetics. *Biophys. J.* **2008**, *95*, 497–502.
- (113) Podgornik, R.; Parsegian, V. A. On a Possible Microscopic Mechanism Underlying the Vapor Pressure Paradox. *Biophys. J.* **1997**, *72*, 942–952.
- (114) Gao, L.; Golubovič, L. Finite-Size Thermomechanical Effects in Smectic Liquid Crystals: The Vapor Pressure Paradox as an Anharmonic Phenomenon. *Phys. Rev. E: Stat. Phys., Plasmas, Fluids, Relat. Interdiscip. Top.* **2003**, *68*, 041907–041932.
- (115) Angelescu, D. G.; Linse, P. Viruses as Supramolecular Self-Assemblies: Modelling of Capsid Formation and Genome Packaging. *Soft Matter* **2008**, *4*, 1981–1990.
- (116) Angelescu, D. G.; Linse, P. Modelling of Icosahedral Viruses. *Curr. Opin. Colloid Interface Sci.* **2008**, *13*, 389–394.
- (117) Angelescu, D. G.; Bruinsma, R.; Linse, P. Monte Carlo Simulations of Polyelectrolytes Inside Viral Capsids. *Phys. Rev. E* **2006**, *73*, 041921–041937.
- (118) Hagan, M. F. Modeling Viral Capsid Assembly. *Adv. Chem. Phys.* **2014**, *155*, 1–68.
- (119) Strey, H. H.; Podgornik, R.; Rau, D. C.; Parsegian, V. A. DNA-DNA Interactions. *Curr. Opin. Struct. Biol.* **1998**, *8*, 309–313.
- (120) French, R.; et al. Long Range Interactions in Nanoscale Science. *Rev. Mod. Phys.* **2010**, *82*, 1887–1944.